



Glucose level monitoring in human blood samples by surface plasmon resonance sensor using cerium oxide and black phosphorus nanomaterials

Vipin Sharma¹ · Lalit Kumar Dwivedi¹ · Sachin Singh² · Ganga Ram Mishra²

Received: 4 October 2023 / Accepted: 9 December 2023
© The Author(s), under exclusive licence to The Optical Society of India 2024

Abstract Diabetes is a chronic metabolic disorder characterized by prolonged elevated blood glucose levels. This research endeavours to assess the efficacy of a surface plasmon resonance (SPR)-based sensor for continuous diabetes monitoring. The proposed sensor structure follows the Kretschmann configuration, incorporating key components such as a prism, Silver/Copper, Cerium Oxide, black phosphorus (BP), and a specialized sensing medium. Within this investigation, two distinct sensor structures, denoted as Structure I and Structure II, have been meticulously constructed using the specified layers. The research employs advanced techniques, including the transfer matrix method and angular interrogation, to evaluate the SPR sensor's performance at a wavelength of 633 nm. The study rigorously analyses the detection capabilities for a specific biological sample, considering parameters such as sensitivity (S), detection accuracy (DA), quality factor (QF), and dip-of-figure of merit (DFOM). Notably, the glucose detection process achieves remarkable results, with Structure I and Structure II exhibiting maximum sensitivities of 217 degree/RIU and 217 degree/RIU, DA values of 0.41 and 0.315, QF values of 89.13 RIU⁻¹ and 68.45 RIU⁻¹, and DFOM values of 31,281.53 and 24,213.34, respectively. Ultimately, this research culminates in a comparative study, underscoring the potential of the proposed sensor as a high-performance tool for glucose level detection, thereby paving new avenues in the realms of biological and biomedical technologies.

Keywords FK51A prism · Glucose · Sensitivity · Optical sensor · Cerium oxide · Transfer matrix method

Introduction

Diabetes is a pervasive health issue that affects millions of individuals worldwide. It poses significant challenges to both individuals and healthcare systems, requiring a multi-disciplinary approach to its management. Diabetes can arise from multiple factors, including genetic predisposition, lifestyle choices, and environmental influences [1]. Diabetes is often divided into two main categories: type 1 diabetes, which is characterized by an autoimmune attack on pancreatic beta cells, and type 2 diabetes, which is caused by insulin resistance and insufficient insulin production. Symptoms of type 1 diabetes, which include increased thirst, frequent urination, unexplained weight loss, and exhaustion, often appear during infancy or adolescence. On the other hand, the symptoms of type 2 diabetes may appear gradually and include increased thirst, hazy vision, sluggish wound healing, and recurring infections. Type 2 diabetes is frequently associated with obesity and sedentary lifestyles. Diabetes can cause serious consequences that impact many different organs and systems, such as heart disease, kidney damage, nerve damage (neuropathy), retinopathy (vision loss), and foot issues, if it is not treated or inadequately controlled. It is crucial to address diabetes promptly to minimize the risk of these complications [2, 3].

Diabetes management requires a multi-faceted approach involving lifestyle modifications, medication, and regular blood glucose monitoring. In order to avoid and control diabetes, it is important to follow a balanced diet, exercise regularly, manage your weight, and de-stress. [4]. Medications such as insulin and oral hypoglycaemic agents are

✉ Lalit Kumar Dwivedi
lalitsln67.2011@gmail.com

¹ Department of Post-Graduate Studies and Research in Physics, Kamla Nehru Institute of Physical & Social Sciences, Sultanpur, Uttar Pradesh, India

² Department of Physics & Electronics, Dr. Rammanohar Lohia Avadh University, Ayodhya, Uttar Pradesh, India

administered based on the specific needs of the individual. Ongoing research focuses on improving the understanding, diagnosis, and treatment of diabetes. The amount of glucose present in a blood sample can be utilized for diagnosing diabetes. Table 1 lists the classifications of diabetes diagnoses.

Monitoring and controlling diabetes as well as the diagnosis of other metabolic illnesses depend on the ability to detect glucose in blood samples. Glucose in blood samples can be detected using various technologies, one of which is surface plasmon resonance. Surface plasmon resonance (SPR) is an optical technique that has revolutionized the field of biophysics and material sciences [5]. By analysing the interaction between light and matter at the nanoscale level, SPR provides valuable insights into the properties and behaviours of materials. One of the primary applications of SPR lies in the field of biochemical sensing. SPR biosensors are used to study biomolecular interactions, helping researchers understand molecular binding events, kinetics, and affinity. With its label-free and real-time monitoring capabilities, SPR has become a powerful tool for studying protein–protein interactions, DNA hybridization, drug discovery, and antibody-antigen interactions [6]. The sensitivity and specificity of SPR make it an invaluable asset for the medical and pharmaceutical industries. In the current theoretical study, the Kretschmann arrangement based on the angular interrogation technique is used [7]. Plasmonic materials like metals are used in the SPR sensor. The two most widely used metals, gold (Au) and silver (Ag), have been utilized to make sensors, although it has been shown that both have weak adherence to prisms [8–13]. To improve adhesion, sensitivity, and other SPR biosensor features, thin coatings of chromium (Cr), Teflon, and indium phosphate have been applied [14]. Copper (Cu) is the most common conductor after silver and is significantly less expensive than gold and silver. Due to its rapid oxidation, Cu has not received much consideration as a plasmonic material. Recently, some researchers [15, 16] suggested that the oxidation problem with metal might be avoided by using appropriate oxide coatings. Particularly among the lanthanum oxides, cerium oxide (CeO_2) is recognized as a significant multifunctional substance due to its usefulness in electromagnetic, electrical, photocatalytic, sensing, and other electromagnetic applications [17–19]. CeO_2 has a wide range

of physical and physical properties, such as semiconductor performance, 3.2 eV band spacing, high oxygen storage capacity, and simple vacant movement due to the ability to transition between Ce^{3+} and Ce^{4+} oxidation states [20, 21]. Cerium oxide nanoparticles are ideal for biomolecule immobilization surfaces because of their thermal and chemical durability, low toxicity, and ease of manufacture [21–27]. According to an experimental study, 2-D materials like black phosphorus (BP) and graphene used as BREs can enhance the sensitivity and performance characteristics of SPR sensors. One of the key features of BP is that, as compared to other 2-D materials, it responds incredibly quickly [28]. This enables it to sense the concentrations of analyte in parts per billion. Graphene, WS_2 , and MoS_2 are all outperformed by graphene in terms of adsorption energy. Additionally, BP has a puckered lattice structure, which gives it a surface-to-volume ratio that is significantly larger than that of other 2D materials [28]. BP may therefore be the best material for molecular binding. Experimental analysis has been done of the BP's electrical and optical characteristics. Cai et al. [29] conducted research indicating that the effective carrier mass, the energy band gap, and the work function exhibits variations in response to changes in the thickness of black phosphorus (BP) material. As the thickness of BP material increases, these parameters change. Notably, black phosphorus has garnered recent recognition as a highly promising medium for various applications owing to its distinctive attributes. These include a direct and customizable band gap, outstanding optical and electrical characteristics, and augmented carrier mobility, as emphasized in [29–31].

The current investigation seeks to optimize the operational characteristics of the surface plasmon resonance (SPR) biosensor for the precise detection of glucose within blood specimens. In this research article, a specialized SPR biosensor configuration, denoted as Prism FK51A/Ag/Cu/ CeO_2 /BP/sensing medium, has been introduced to offer an elevated level of sensitivity. This study encompasses a comprehensive assessment of all pertinent performance metrics, which have been meticulously evaluated and computationally simulated through the utilization of MATLAB 2019 software.

Device structure and methodology

The fundamental illustration of the proposed multi-layer biosensor employing a Kretschmann configuration is depicted in Fig. 1. The structure comprises six distinct layers, sequentially arranged as follows: FK51A Prism/Metal/ CeO_2 /BP/Sensing media. To optimize the performance characteristics of this biosensor, all layers are meticulously engineered to possess nanometre-scale thicknesses (nm), with a working wavelength of 633 nm. Specifically, the initial layer is

Table 1 Classification of diabetes

Category	Glucose levels in the blood after a meal (mM)
Healthy	< 8.0
Pre-diabetes	7.80–11.10
Diabetes	> 11.110

Fig. 1 Basic diagram of proposed SPR sensor

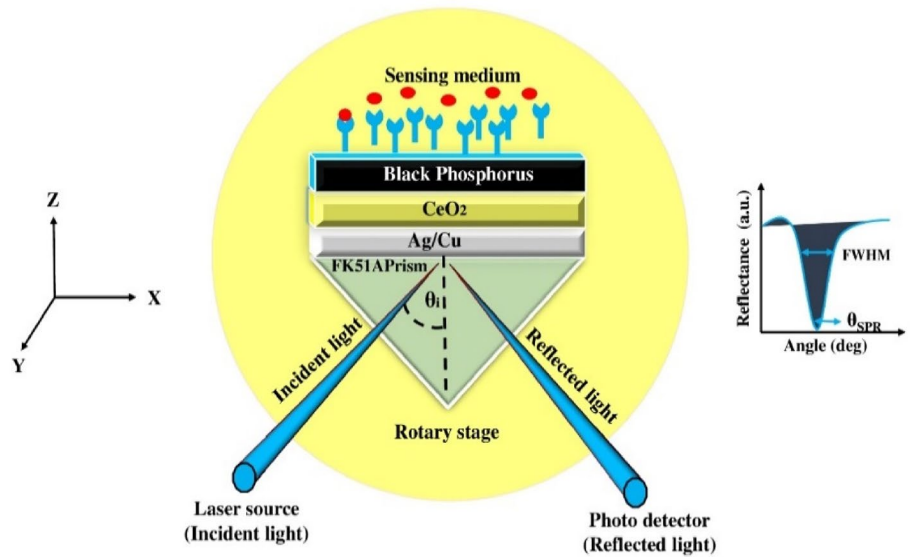


Table 2 RI for different glucose concentrations

Glucose concentration		Refractive index (RIU)
00.0 mM	0.00%	1.3391
07.00 mM	0.13%	1.3481
12.00 mM	0.22%	1.3572
17.00 mM	0.31%	1.3671
22.00 mM	0.40%	1.3765
55.50 mM	1.00%	1.3853
111.0 mM	2.00%	1.3940
166.60 mM	3.00%	1.4014

fashioned from FK51A glass as a prism. To compute the refractive index of this prism, Eq. (1) can be employed, with λ denoting the wavelength in (μm) [32].

$$n_p = \left(1 + \frac{0.971247817\lambda^2}{\lambda^2 - 0.00472301995} + \frac{0.21690141\lambda^2}{\lambda^2 - 0.0153575612} + \frac{0.904651666\lambda^2}{\lambda^2 - 168.68133} \right)^{1/2} \quad (1)$$

A thin layer of CeO_2 with a thickness of $d_2 = 6$ nm for structure-I and 1 nm for structure-II -II and a thin layer of BP with a thickness of $d_3 = 0.53$ nm have been placed on top of the thin layer of Ag/Cu that coats the prism’s base. In a case study, BP is used over the CeO_2 layer to effectively detect efficient glucose in blood samples. Based on the data of people with diabetes disease, as shown in Table 2, we calculated the change in glucose concentration in this study. The RI values at various glucose concentrations were calculated using linear fitting of experimental data from earlier research [33]. The simulation starts with a baseline glucose concentration

Table 3 Values of λ_p and λ_c for Cu and Ag

Metal	Plasma wavelength (λ_p)	Collision wavelength (λ_c)	References
Cu	1.3617×10^{-7} mt	4.0853×10^{-7} mt	[16]
Ag	1.4541×10^{-7} mt	1.7614×10^{-7} mt	[35]

of 0.00 mM. Humans in good health are considered to have blood glucose levels of 7.00 mM (00.130%), while those with diabetes are considered to have blood glucose levels of 12.00 mM (00.220%) and 17.00 mM (00.310%). Here also include the variation for higher glucose concentrations, namely 22.00 mM (0.40%), 55.50 mM (1%), 111.00 mM (2%), and 166.60 mM (3%), in order to check the stability of the sensors.

The complex refractive index of metal layers has been determined using the Drude-Lorentz model using Eq. 2 [34].

$$n^2 = \left(1 - \frac{\lambda^2 \lambda_c}{\lambda_p^2 (\lambda_c + i\lambda)} \right) \quad (2)$$

where λ , λ_p , and λ_c represent distinct parameters: λ signifies the operational wavelength associated with the monochromatic light source, while λ_p and λ_c signifies the plasma and collision wavelengths, respectively (Table 3).

The material CeO_2 has an optimized thickness of 6 nm for structure I and 1 nm for structure II and a refractive index of 2.2. Black phosphorus (BP) has an optimized thickness of 0.53 nm and a refractive index of $3.50 + i \cdot 0.01$. Our structure can be summed up as follows: the first layer is a prism made of FK51A glass to couple the entire incident light, the second layer is a metal (Ag/Cu) layer to produce surface plasmons at the interface, the third layer is CeO_2 to enhance

the plasmonic effects and protect the metal against oxidation, and the fourth is BP to further enhance the sensing performance of the biosensor.

Theoretical modelling of the proposed biosensor

The subsequent methodologies are available for the numerical evaluation of optical attributes, encompassing transmittance and reflectance, within the context of a complex multi-layer thin film nanostructure apparatus: (a) Resultant Wave Method (b) Field Element Method (c) Transfer Matrix Method (TMM). The transfer matrix method (TMM) offers significant advantages, including exceptional accuracy, inherent simplicity, and a complete absence of approximation. Consequently, in the present study, the mathematical analysis of the N-layer model is done using the transfer matrix method (TMM) and Fresnel equations. This comprehensive approach facilitates the in-depth characterization of the electromagnetic field at both the initial and last surfaces along the tangential direction, as articulated as follows: [11]

$$\frac{H_1}{P_1} = A_{ij} \left[\frac{H_{N-1}}{P_{N-1}} \right] \tag{3}$$

where H_1 and H_{N-1} represent the tangential components of magnetic fields, while P_1 and P_{N-1} denote the tangential components of electric fields for the first and Nth surface. A is denoted as the characteristic's matrix for the amalgamated structure, which is derived through the following mathematical equation:

$$A = \prod_{k=2}^N A_k = \begin{vmatrix} A_{11} & A_{12} \\ A_{21} & A_{22} \end{vmatrix} \tag{4}$$

$$A_k = \begin{vmatrix} \cos \beta_k & -i \sin \beta_k / q_k \\ -i \sin \beta_k & \cos \beta_k \end{vmatrix} \tag{5}$$

Here β_k and q_k are

$$q_k = \frac{(\epsilon_k - n^2 \sin^2 \theta_1)^{1/2}}{\epsilon_k}, \beta_k = \frac{2\pi d_k}{\lambda} = (\epsilon_k - n^2 \sin^2 \theta_1)^{1/2}$$

where θ_1 represents the angle of incidence, while λ denotes the wavelength of incident light. Additionally, d_k signifies the thickness of the kth layer, and ϵ_k represents the dielectric constant of the kth layer. The total reflection coefficient of p-polarized light (r_p) is determined as follows:

$$r_p = \frac{(A_{11} + A_{12}X_N)X_1 - (A_{21} + A_{22}X_N)}{(A_{11} + A_{12}X_N)X_1 + (A_{21} + A_{22}X_N)} \tag{6}$$

The reflectivity of the given multi-layer configuration is given by

$$R_p = |r_p|^2 \tag{7}$$

Performance parameter

The evaluation of the performance of the surface plasmon resonance (SPR) sensor encompasses a various pivotal parameter. These parameters encompass the assessment of sensitivity (S), the measurement of the full width at half maximum (FWHM), the determination of detection accuracy (DA), and the calculation of figures of merit (FOM).

Sensitivity

The angular sensitivity is formally defined as the ratio of the change in the SPR angle ($\Delta\theta_{res}$) to the alteration in refractive index (Δn). This parameter quantifies how variations in the refractive index impact the shift in the surface plasmon resonance (SPR) angle and is given as follows:

$$S = \frac{\Delta\theta_{res}}{\Delta n} \tag{8}$$

Full width at half maxima (FWHM)

The full width at half maximum (FWHM) value serves as a critical indicator of the reflectance curve's degree of sharpness. A multitude of parameters, including detection accuracy (DA) and quality factor (QF), rely on the FWHM for their calculation, establishing it as a pivotal component in the analysis. Minimizing the FWHM value is imperative, as it contributes to enhancing the precision of various measurements. FWHM is formally defined as the width of the curve at half of its maximum amplitude and given as follows:

$$FWHM = \theta_1 - \theta_2 \tag{9}$$

Detection accuracy

It is commonly referred to as the signal-to-noise ratio (SNR). Detection Accuracy exhibits an inverse correlation with the full width at half maximum (FWHM) and is formally characterized as:

$$DA = \frac{1}{FWHM} \tag{10}$$

Quality factor

The quality factor (Q) is formally expressed as the ratio of Sensitivity to the full width at half maximum (FWHM), and it is denoted as:

$$QF = \frac{S}{FWHM} \tag{11}$$

Dip of figure of merit

The dip of the Figure of Merit is formally described as the ratio of Sensitivity to Minimum Reflectance.

$$DFOM = \frac{S}{\text{MinimumReflectance}} \tag{12}$$

Results and discussion

Optimization of layers thickness for SPR structure

This section studied the optimal thickness of the Ag/Cu and CeO₂ layers, as their performance is influenced by the

characteristics of the upper dielectric material. The focus of this optimization lies in achieving the lowest possible value for R_{\min} [10]. A lower R_{\min} signifies enhanced light energy transfer to the surface plasmon waves (SPW), consequently enhancing surface plasmon resonance (SPR) performance. Our research encompasses two distinct structures, referred to as structure-I and structure-II, with their respective configurations outlined in Table 4 (Fig. 2).

Performance analysis of prism-based structures: optimized Ag/Cu thickness

In conventional surface plasmon resonance (SPR) structures, the primary focus of optimization on the thickness of Ag/Cu layers and the coupling prism. Figure 3 provides a visual representation of the structural characteristics in a typical SPR configuration (FK51A Prism-Ag/Cu-sensing) with varying metal thicknesses, spanning from 35 to 55 nm with 5 nm increments. These graphical representations demonstrate asymmetry due to alterations in layer thickness and the spatial expansion of surface plasmons (SPs) within the surrounding medium. The minimum reflectance value (R_{\min}) reaches its lowest point at a Cu thickness of 55 nm, registering at 0.0093, while a value of 0.001361 is observed at the Ag thickness, albeit with an increase in subsequent measurements. This reduction in R_{\min} can be attributed to minimal absorption loss and the extended spatial reach of SPs, influenced by their propagation length (PL) in the parallel direction. In summary, the optimal thickness for Cu and Ag layers in conventional SPR sensors is identified as 55 nm, effectively facilitating the excitation of higher-order SPs. The parameter denoted as 'S,' computed using Eq. (8), yields values of 141.57 degree/RIU and 129.51 degree/RIU.

Table 4 Different Structures number, name, and configurations

Structure number	Name	Configuration
I	Cu-CeO ₂ -BP based SPR	Cu-CeO ₂ -BP-sensing medium
II	Ag-CeO ₂ -BP based SPR	Cu-CeO ₂ -BP-sensing medium

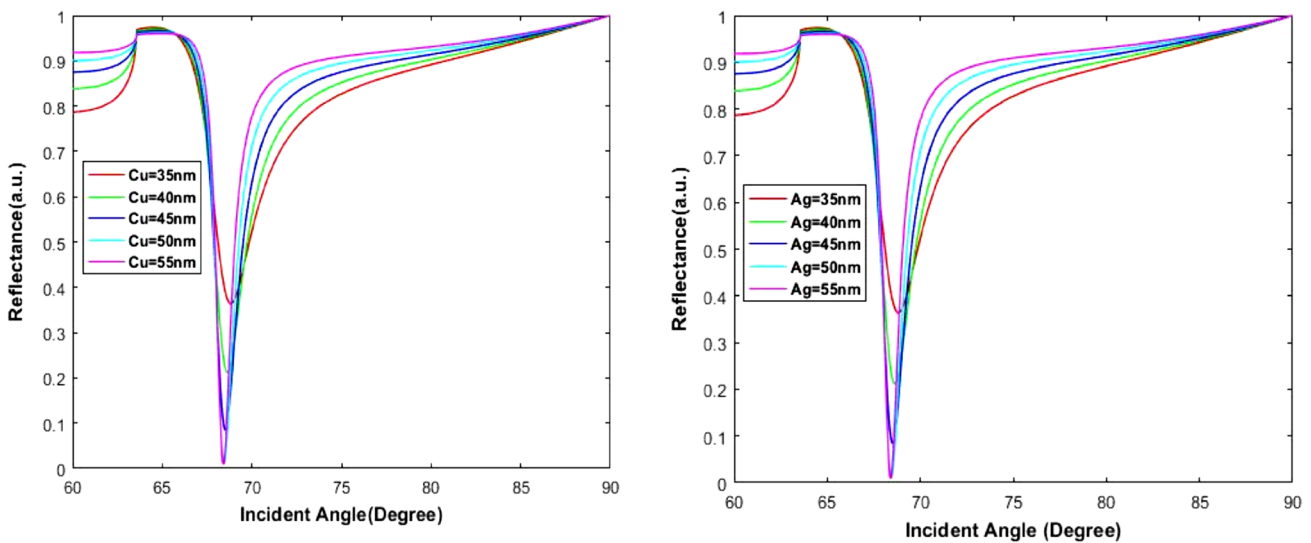


Fig. 2 Reflectance versus angle for different metal film thickness to obtain optimized metal Ag and Cu thicknesses

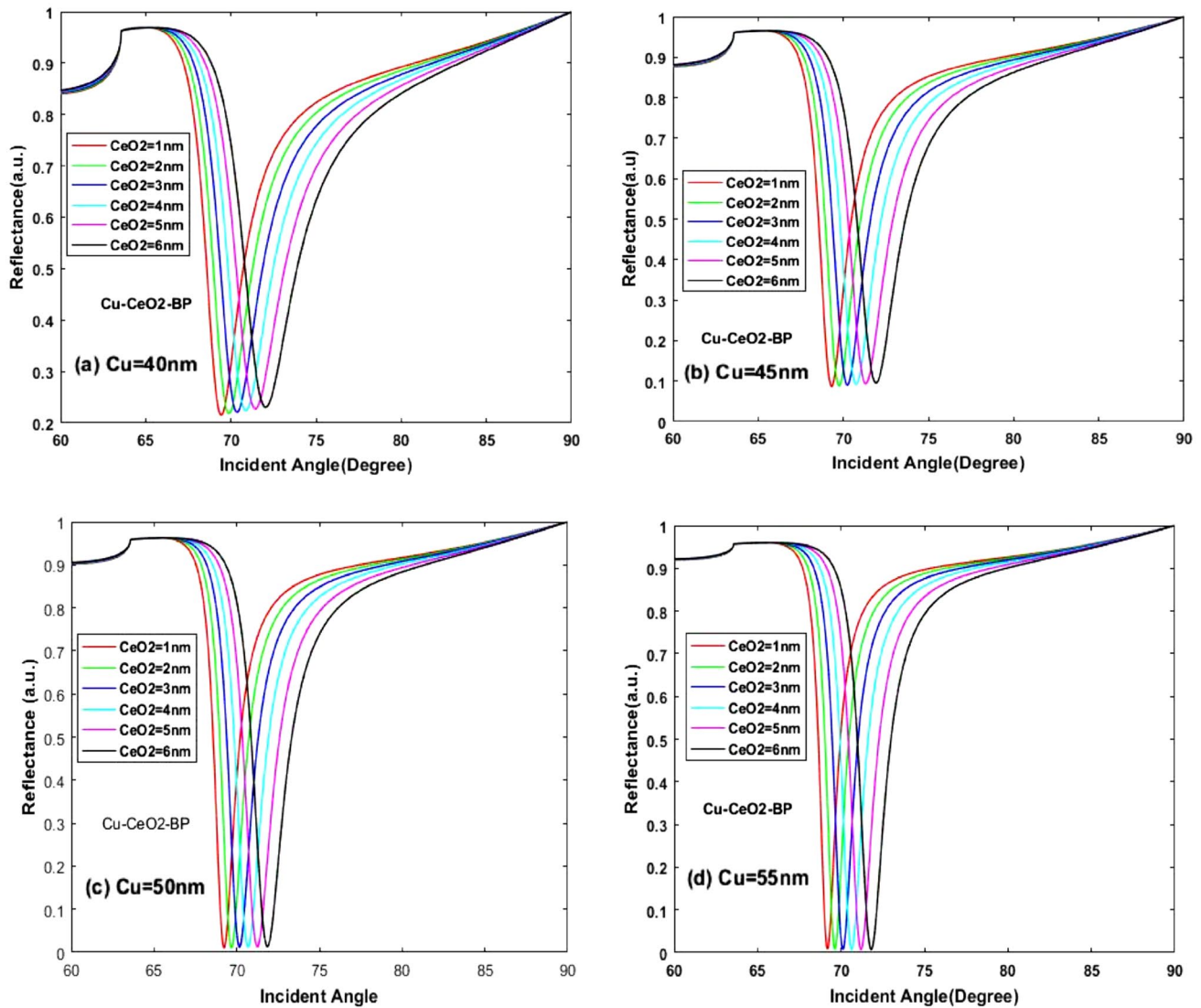


Fig. 3 Using angular interrogation, the reflectance curves of a Cu-CeO₂-BP based structure for various CeO₂ layer thicknesses at various Cu a thickness of **a** of 40 nm, **b** of 45 nm, **c** of 50 nm, and **d** of 55 nm

Optimization of Cu, CeO₂ thickness for Cu-CeO₂-BP structure-I

The detection technique depends on the optimized structure, hence in this section, structure-I is used to optimize the Cu and CeO₂ thicknesses. The structure-I's reflectance curves are shown in Fig. 3 for different Cu thicknesses (Cu: 40 to 55 nm with an interval of 5 nm) and for different CeO₂ layer thicknesses (CeO₂: 1 to 6 nm with an interval of 1 nm). Fig. 3a for Cu of 40 nm, Fig. 3b for Cu of 45 nm, Fig. 3c for Cu of 50 nm, Fig. 3d for Cu of 55 nm. Due to its low absorption loss, the thickness of the BP layer in this section is kept constant at 0.53 nm. The variations in layer thickness that affect the SP's excitations, penetration depth,

and penetration length of the sensor, the resonance dip and R_{\min} of the SPR curves in Fig. 3 are asymmetrical. Table 5 includes the R_{\min} values that were acquired for Fig. 3. Less R_{\min} is furnished at Cu and CeO₂ thicknesses of 55 nm and 6 nm, respectively. As a result, these optimized thicknesses are used to analyse structure-I for the detection of certain biological samples.

Optimization of Ag, CeO₂ thickness for Ag-CeO₂-BP structure-II

Similar reflectance curves for the structure II are shown in Fig. 4 in terms of an angle. The Ag and CeO₂ thicknesses in this case are varied (Ag: 40–55 nm with a 5 nm interval, and CeO₂: 1–6 nm with a 1 nm interval). The obtained R_{\min}

Table 5 Measurement of R_{\min} values of various Cu and CeO₂ thickness of structure I

Cu Thickness	R_{\min} values for various CeO ₂ thicknesses					
	1 nm	2 nm	3 nm	4 nm	5 nm	6 nm
Cu=40 nm	0.2157	0.2184	0.2212	0.2242	0.2273	0.2304
Cu=45 nm	0.08641	0.08808	0.08983	0.09165	0.09352	0.0954
Cu=50 nm	0.01068	0.01122	0.01179	0.01239	0.013	0.01361
Cu=55 nm	0.008921	0.008507	0.008093	0.007687	0.007297	0.006937

values for Fig. 4 a-d are reported in Table 6, where it is found that the Ag and CeO₂ thicknesses of 50 nm and 1 nm, respectively, have the lowest R_{\min} values. To explore structure-II for the detection of biological samples, these optimized thicknesses are used. In summary, the thicknesses of Ag are 50 nm and CeO₂ is 1nm.

Performance analysis of glucose level in blood sample

In the analysis of glucose level detection in blood samples, we have plotted reflectance curves for two distinct structures, as depicted in Fig. 5. Figure 5a represents structure-I,

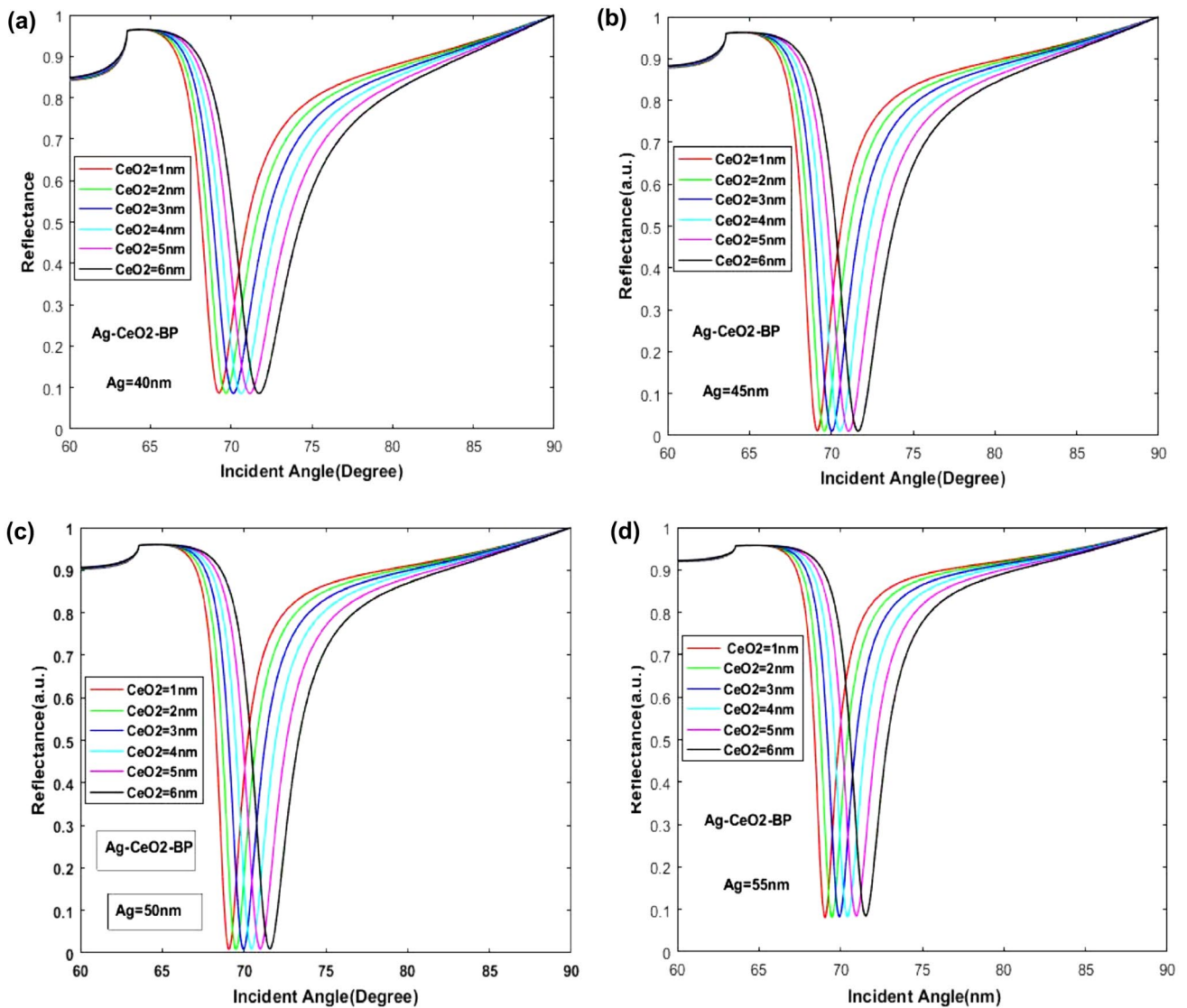


Fig. 4 Ag-CeO₂-BP based structure’s reflectance curves using angular interrogation for various CeO₂ layer thicknesses at different Ag Thickness **a** Ag of 40 nm **b** Ag of 45 nm **c** Ag of 50 nm **d** Ag of 55 nm

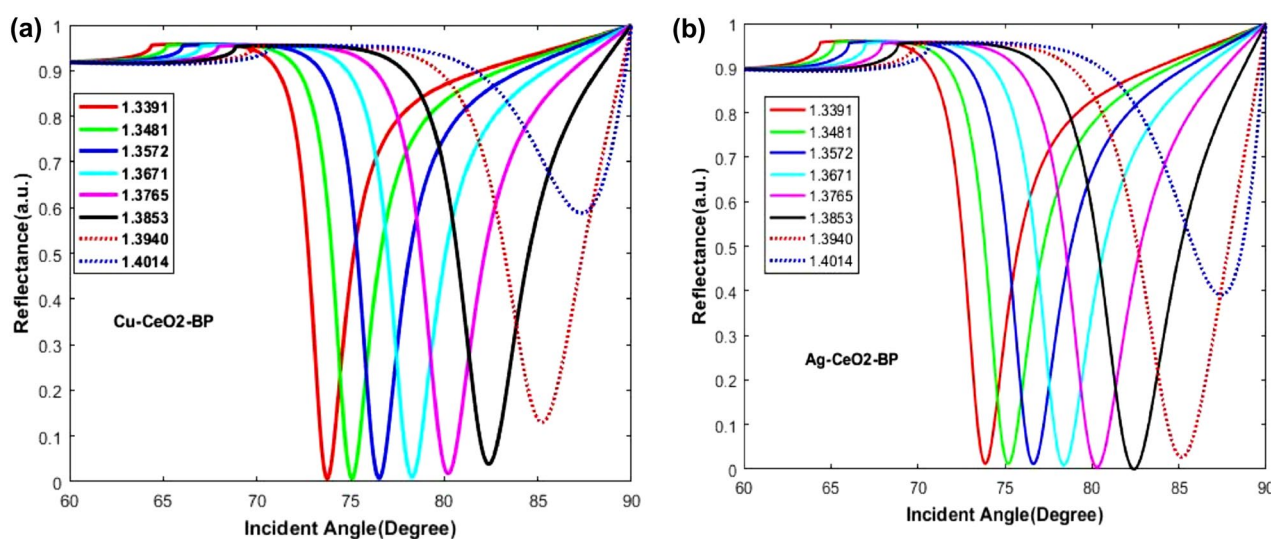
Table 6 Measurement of R_{\min} values of various Ag and CeO_2 thickness of structure-II

Ag Thickness	R_{\min} values for various CeO_2 thicknesses					
	1 nm	2 nm	3 nm	4 nm	5 nm	6 nm
Ag= 40 nm	0.0867	0.08642	0.8621	0.08607	0.08598	0.08591
Ag= 45 nm	0.01068	0.01048	0.01031	0.01031	0.01016	0.009885
Ag= 50 nm	0.008962	0.009212	0.009445	0.009667	0.009885	0.01011
Ag= 55 nm	0.08087	0.08169	0.08247	0.08323	0.08398	0.08477

while Fig. 5b pertains to structure-II. These curves exhibit non-symmetrical SPR resonance dips, full width at half maximum (FWHM), and R_{\min} values due to the excitation of surface plasmons (SPs) at the interface between the prism and the metal layer, coupled with variations in the refractive index (RI) of the sensing medium. The achieved sensitivity for blood glucose detection is remarkable, measuring 217 deg/RIU for both structure-I and structure II. Furthermore, the obtained FWHMs for structure-I and structure-II are 2.42 degrees and 2.3 degrees, respectively. Additionally, we have computed detection accuracy (DA), quality factor (QF), and dip-of-figure of merit (DFOM) using Eqs. 10–12, respectively. For structure-I, the results are DA of 0.41, QF of 89.13 RIU⁻¹, and DFOM of 31,281.53, while for structure-II, we observe DA of 0.315, QF of 68.45 RIU⁻¹, and DFOM of 24,213.34. The comprehensive performance analysis highlights that structure I and II are both effective in detecting glucose levels in the blood, offering impressive sensitivity (S), quality factor (QF), detection accuracy (DA), and dip-of-figure of merit (DFOM).

Effect of the number of BP layers

The variations in the number of BP (Black Phosphorus) layers at specific thicknesses, with Cu at 55 nm and Ag at 50 nm, are depicted in Fig. 6a and 6b. These variations in BP layers correspondingly alter the resonance angle. Consequently, there is an observable shift in the dip of the reflectance curve, resulting in an enhancement of the optimized angular sensitivity for the proposed surface plasmon resonance (SPR) sensor. This improvement extends to other performance parameters, including detection angle (DA), quality factor (QF), and detection figure of merit (DFOM). In Fig. 7a and 7b, the sensitivity of a monolayer of BP, with a fixed thickness of 50 nm for Ag and 55 nm for Cu, is detailed. Structure-I exhibits a sensitivity of 209 degrees/RIU, while structure-II registers 151 degrees/RIU. For structure-I, the angular sensitivity increases from 209 degrees/RIU to a peak of 217 degrees/RIU with the addition of BP layers, similarly increasing from 151 degrees/RIU to 217 degrees/RIU for structure-II. The optimized angular sensitivity is prominently depicted in Fig. 7a at 209 degrees/RIU for the monolayer but reaches a maximum of 217 degrees/RIU for structure-I at the bilayer stage, gradually declining

**Fig. 5** Reflectance curves using angular interrogation for different RIs of Glucose concentration in blood samples **a** Cu-CeO₂-BP **b** Ag-CeO₂-BP

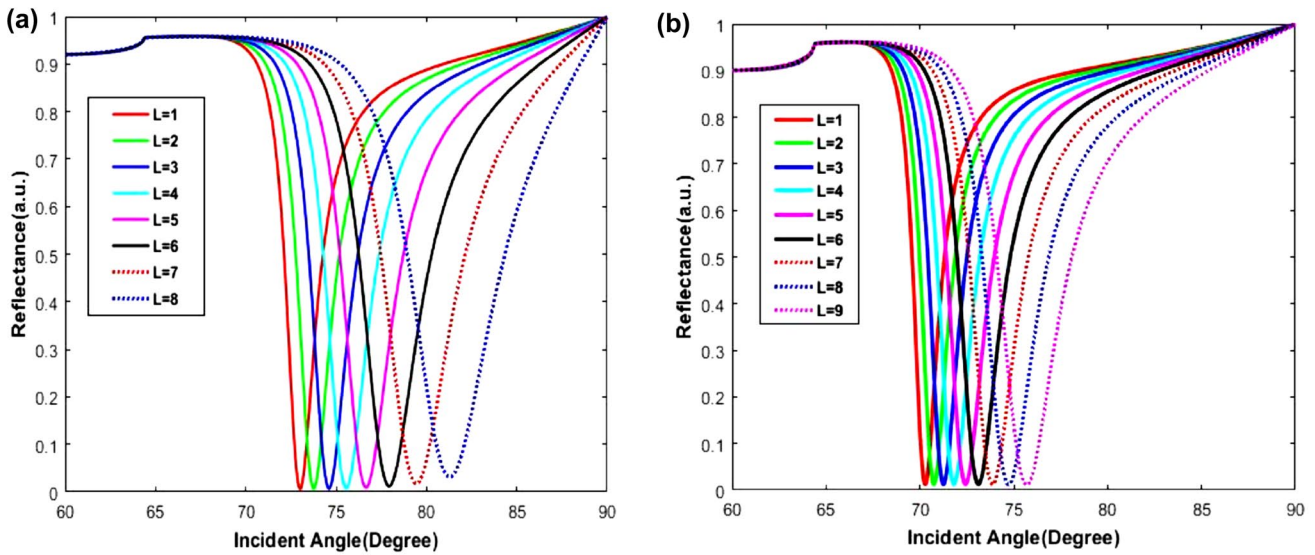


Fig. 6 Reflectivity curve variation for different numbers of BP layers **a** Structure-I **b** Structure-II

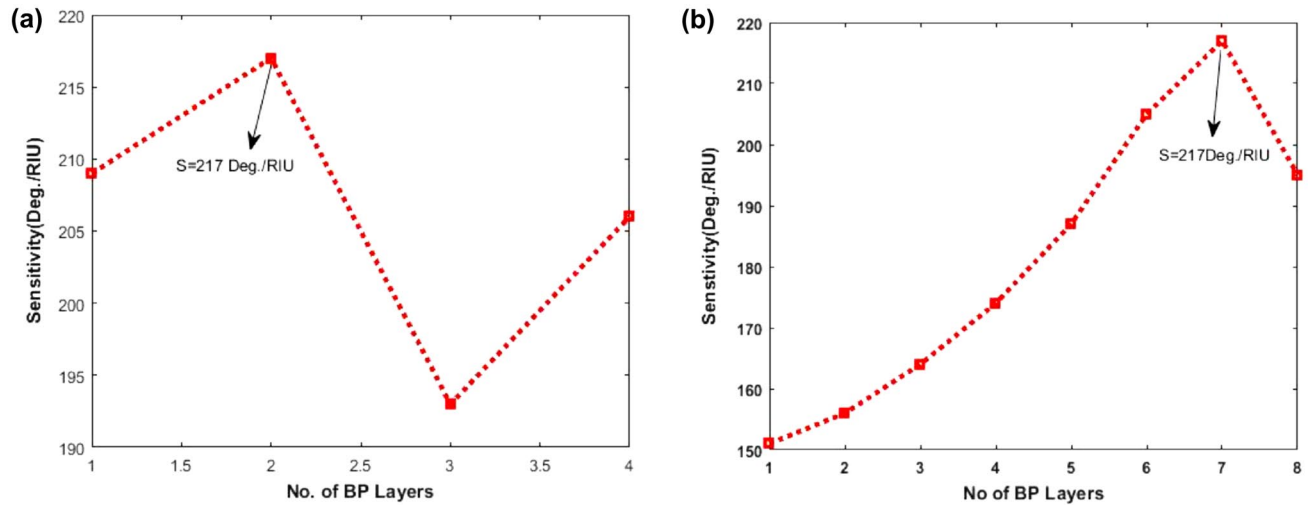


Fig. 7 Sensitivity variations with different number of BP layers for the Proposed SPR sensor

thereafter. Figure 7b illustrates that the monolayer’s optimized angular sensitivity is 151 degrees/RIU, whereas for structure-II, it attains a maximum of 217 degrees/RIU with seven layers before gradually decreasing. Consequently, the maximum angular sensitivity for both structures I and II are 217 degrees/RIU.

Comparative study on performance analysis

In this section, we have conducted a comprehensive evaluation of the proposed sensor’s performance in comparison to prior research efforts conducted by fellow researchers, as evidenced in Table 7. Our study reveals that the proposed approach, involving both structure-I and structure-II,

exhibits enhanced capabilities in terms of sensitivity (S) and detection accuracy (DA) when compared to previously conducted work. Notably, our system achieves superior performance in the vital task of blood glucose level detection, with a sensitivity (S) of 217 degrees/RIU and 0.41 for structure I, and 217 degrees/RIU and 0.43 for structure II. Furthermore, our research marks a significant milestone by shedding light on the impressive performance of quality factor (QF) and detection figure of merit (DFOM) in the context of specific biological sample detection, a dimension not explored in previous studies. This heightened performance is quantified with a quality factor (QF) of 89.13 RIU⁻¹ and the detection figure of merit (DFOM) of 31,281.53 for structure-I, while structure-II achieves the quality factor (QF) of 75.65 RIU⁻¹

Table 7 The performance of the proposed work and existing work comparison on the detection of glucose in blood samples

Reference	Structure	Detection of glucose level in a blood sample			
		S (deg/RIU)	DA	QF (RIU ⁻¹)	DFOM
Nurgroho et al. [31]	Prism (BK7)-Cr-Au-Sensing Medium	116.69	–	–	–
Proposed work	Prism (FK51A)-Cu-CeO ₂ -BP-Sensing Medium	217	0.41	89.13	31,281.53
Proposed work	Prism (FK51A)-Ag-CeO ₂ -BP-Sensing Medium	217	0.315	68.45	24,213.34

and a detection figure of merit (DFOM) of 19,415.30. These results underscore the remarkable advancements made in our research, showcasing the potential for significantly improved detection processes in the realm of biological samples.

Conclusions

This study presents a novel numerical modelling approach for a surface plasmon resonance (SPR) sensor designed specifically for precise glucose level measurement. The sensor utilizes a unique "Ag/Cu-CeO₂-BP" structure in conjunction with an FK51A prism, employing two distinct structural configurations known as structure-I and structure-II, both incorporating the specified materials. The assessment of the sensor's performance revolves around critical parameters, including "sensitivity (S)," "detection accuracy (DA)," "quality factor (QF)," and the innovative inclusion of "dip-of-figure of merit (DFOM)". Collectively, these metrics provide a comprehensive evaluation of the sensor's efficacy in detecting biological samples.

Notably, both structure-I and structure-II exhibit exceptional Sensitivity, registering 217 deg/RIU, indicative of their capability to discern even subtle changes in refractive index units (RIU). In terms of detection accuracy (DA), structure-I achieves a commendable 0.41, while structure-II closely follows with a value of 0.315, confirming their reliability in accurately measuring glucose levels. Moreover, the quality factor (QF) analysis underscores the efficiency of these structures, with structure-I achieving a high QF of 89.13 RIU⁻¹ and structure-II demonstrating a respectable QF of 68.45 RIU⁻¹. The study introduces the novel concept of dip-of-figure of merit (DFOM), further enriching the sensor's performance assessment. Structure-I exhibits a DFOM of 31281.53, while structure-II showcases a DFOM of 24213.34, highlighting their superior capabilities.

Furthermore, a comprehensive comparative analysis reveals significant enhancements in sensitivity (S) and detection accuracy (DA) when compared to prior research, solidifying the innovative contributions of this study. The inclusion of quality factor (QF) and dip-of-figure of merit (DFOM) as evaluation criteria represents a pioneering advancement in SPR sensor technology. Consequently, this

research introduces a cutting-edge numerical modelling approach for an SPR sensor featuring the "Ag/Cu-CeO₂-BP" structure, tailored for precise glucose level measurement. With outstanding Sensitivity, Detection Accuracy, Quality Factor, and the pioneering inclusion of Dip-of-Figure of Merit, this sensor presents a promising and high-performance solution for the precise detection of biological materials. Its potential applications extend to the fields of biomedical and biological research, offering an innovative platform for advanced diagnostics and analyses in these critical domains.

Acknowledgements This research does not receive any specific grant from funding agencies in the public, commercial, or not-for-profit.

Author contribution VS: Original draft writing, methodology, conceptualization, software work, LKD: Supervision, SS: reviewing, editing and GRM: revising the manuscript.

Declarations

Conflict of interest The authors declare no competing interests.

Ethics approval This is a theoretical study that does not require ethical approval.

Conflict of interest The authors do have not any conflict of interest.

References

1. American Diabetes Association, Classification and diagnosis of diabetes. *Diabetes Care* **38**, S8–S16 (2015). <https://doi.org/10.2337/dc15-S005>
2. J. Aakko, T. Uomilehto, J. Aana, L. Indström, J. Ohan, G.E. Riksson, I.T.V. Alle, E.H. Ämäläinen, L.-P. Arikka, S. Irkka K Einänen-K Iukaanniemi, M. Auri, L. Aakso, A. Nne, L. Ouheranta, M. Erja, R. Astas, V. Irpi, S. Alminen, M. Atti, A. Bstract, Prevention of type 2 diabetes mellitus by changes in lifestyle among subjects with impaired glucose tolerance. *N. Engl. J. Med.*, **344**(3): 1343–1350 (2001)
3. R. Varma, N.M. Bressler, Q.V. Doan, M. Gleeson, M. Danese, J.K. Bower, E. Selvin, C. Dolan, J. Fine, S. Colman, A. Turpcu, Prevalence of and risk factors for diabetic macular edema in the United States. *JAMA Ophthalmol.* **132**(11), 1334–1340 (2014). <https://doi.org/10.1001/jamaophthalmol.2014.2854>
4. P. Anastas, N. Eghbali, Green chemistry: principles and practice. *Chem. Soc. Rev.* **39**(1), 301–312 (2010). <https://doi.org/10.1039/b918763b>

5. J. Homola, Surface plasmon resonance sensors for detection of chemical and biological species. *Chem. Rev.* **108**(2), 462–493 (2008). <https://doi.org/10.1021/cr068107d>
6. J. Homola, M. Piliarik, *Surface plasmon resonance (SPR) sensors* (Springer Berlin Heidelberg, 2006), pp.45–67. https://doi.org/10.1007/5346_014
7. A.P. Vinogradov, A.V. Dorofeenko, A.A. Pukhov, A.A. Lisyansky, Exciting surface plasmon polaritons in the Kretschmann configuration by a light beam. *Phys. Rev. B* (2018). <https://doi.org/10.1103/PhysRevB.97.235407>
8. S. Pal, A. Verma, Y.K. Prajapati, J.P. Saini, Sensitive detection using heterostructure of black phosphorus, transition metal di-chalcogenides, and MXene in SPR sensor. *Appl. Phys. A Mater. Sci. Process.* (2020). <https://doi.org/10.1007/s00339-020-03998-1>
9. R. Jha, A.K. Sharma, Design of a silicon-based plasmonic biosensor chip for human blood-group identification. *Sens. Actuators B Chem.* **145**(1), 200–204 (2010). <https://doi.org/10.1016/j.snb.2009.11.060>
10. S. Pandey, S. Singh, S. Agarwal, A.K. Sharma, P. Lohia, D.K. Dwivedi, Simulation study to improve the sensitivity of surface plasmon resonance sensor by using ferric oxide, nickel and antimonene nanomaterials. *Optik* **267**, 169757 (2022). <https://doi.org/10.1016/j.ijleo.2022.169757>
11. V. Yesudasu, H.S. Pradhan, R.J. Pandya, Recent progress in surface plasmon resonance-based sensors: a comprehensive review. *Heliyon* (2021). <https://doi.org/10.1016/j.heliyon.2021.e06321>
12. X. Dai, Y. Liang, Y. Zhao, S. Gan, Y. Jia, Y. Xiang, Sensitivity enhancement of a surface plasmon resonance with tin selenide (SnSe) allotropes. *Sensors (Switzerland)* (2019). <https://doi.org/10.3390/s19010173>
13. V.E. Bochenkov, M. Frederiksen, D.S. Sutherland, Enhanced refractive index sensitivity of elevated short-range ordered nano-hole arrays in optically thin plasmonic Au films. *Opt. Express* **21**(12), 14763 (2013). <https://doi.org/10.1364/oe.21.014763>
14. X.C. Yuan, B.H. Ong, Y.G. Tan, D.W. Zhang, R. Irawan, S.C. Tjin, Sensitivity-stability-optimized surface plasmon resonance sensing with double metal layers. *J. Opt. A Pure Appl. Opt.* **8**(11), 959–963 (2006). <https://doi.org/10.1088/1464-4258/8/11/005>
15. S. Singh, S.K. Mishra, B.D. Gupta, Sensitivity enhancement of a surface plasmon resonance-based fiber optic refractive index sensor utilizing an additional layer of oxides. *Sens. Actuators A* **193**, 136–140 (2013). <https://doi.org/10.1016/j.sna.2013.01.012>
16. J.N. Nur, M.H.H. Hasib, F. Asrafy, K.N. Shushama, R. Inum, M.M. Rana, Improvement of the performance parameters of the surface plasmon resonance biosensor using Al₂O₃ and WS₂. *Opt. Quant. Electron.* (2019). <https://doi.org/10.1007/s11082-019-1886-9>
17. M.G. Daher, S.A. Taya, I. Colak, S.K. Patel, M.M. Olaimat, O. Ramahi, Surface plasmon resonance biosensor based on graphene layer for the detection of waterborne bacteria. *J. Biophotonics* (2022). <https://doi.org/10.1002/jbio.202200001>
18. G. Seong, M. Dejhoseini, T. Adschiri, A kinetic study of catalytic hydrothermal reactions of acetaldehyde with cubic CeO₂ nanoparticles. *Appl. Catal. A General* **550**, 284–296 (2017). <https://doi.org/10.1016/j.apcata.2017.11.023>
19. T.K. Mishra, A. Kumar, S.K. Sinha, B. Gupta, Wear behavior and XRD analysis of reinforced copper matrix composite reinforced with cerium oxide (CeO₂). *Bhupendra Gupta Mater. Today Proc.* **5**(14), 27786–27794 (2018)
20. S. Singh, P.K. Singh, A. Umar, P. Lohia, H. Albargi, L. Castañeda, D.K. Dwivedi, 2D nanomaterial-based surface plasmon resonance sensors for biosensing applications. *Micromachines* **11**(8), 779 (2020). <https://doi.org/10.3390/mi11080779>
21. S. Sebastiammal, A. Mariappan, K. Neyvasagam, A.L. Fathima, *Annona muricata* inspired synthesis of CeO₂ nanoparticles and their antimicrobial activity. *Mater. Today Proc.* **9**, 627–632 (2018). <https://doi.org/10.1016/j.matpr.2018.10.385>
22. K. Fugane, T. Mori, D.R. Ou, P. Yan, F. Ye, H. Yoshikawa, J. Drennan, Improvement of cathode performance on Pt-CeOx by optimization of electrochemical pre-treatment condition for PEFC application. *Langmuir* **28**(48), 16692–16700 (2012). <https://doi.org/10.1021/la302912>
23. H.R. Pouretedal, Z. Tofangsazi, M.H. Keshavarz, Photocatalytic activity of mixture of ZrO₂/SnO₂, ZrO₂/CeO₂ and SnO₂/CeO₂ nanoparticles. *J. Alloys Compd.* **513**, 359–364 (2012). <https://doi.org/10.1016/j.jallcom.2011.10.049>
24. Y. Wang, B. Li, C. Zhang, L. Cui, S. Kang, X. Li, L. Zhou, Ordered mesoporous CeO₂-TiO₂ composites: Highly efficient photocatalysts for the reduction of CO₂ with H₂O under simulated solar irradiation. *Appl. Catal. B* **130–131**, 277–284 (2013). <https://doi.org/10.1016/j.apcatb.2012.11.011>
25. K. Hamidian, A. Najafidoust, A. Miri, M. Sarani, Photocatalytic performance on degradation of Acid Orange 7 dye using biosynthesized un-doped and Co doped CeO₂ nanoparticles. *Mater. Res. Bull.* (2021). <https://doi.org/10.1016/j.materresbull.2021.111206>
26. M. Sun, Z. Li, H. Li, Z. Wu, W. Shen, Y.Q. Fu, Mesoporous Zr-doped CeO₂ nanostructures as superior supercapacitor electrode with significantly enhanced specific capacity and excellent cycling stability. *Electrochim. Acta* (2020). <https://doi.org/10.1016/j.electacta.2019.135366>
27. M. Wang, M. Shen, X. Jin, J. Tian, Y. Shao, L. Zhang, Y. Li, J. Shi, Exploring the enhancement effects of hetero-metal doping in CeO₂ on CO₂ photocatalytic reduction performance. *Chem. Eng. J.* (2022). <https://doi.org/10.1016/j.cej.2021.130987>
28. N. Mao, J. Tang, L. Xie, J. Wu, B. Han, J. Lin, S. Deng, W. Ji, H. Xu, K. Liu, L. Tong, J. Zhang, Optical anisotropy of black phosphorus in the visible regime. *J. Am. Chem. Soc.* **138**(1), 300–305 (2016). <https://doi.org/10.1021/jacs.5b10685>
29. S. Srivastava, S. Singh, A.C. Mishra, P. Lohia, D.K. Dwivedi, Numerical study of titanium dioxide and mxene nanomaterial-based surface plasmon resonance biosensor for virus sars-cov-2 detection. *Plasmonics* (2023). <https://doi.org/10.1007/s11468-023-01874-1>
30. M. Pandaram, S. Santhanakumar, R. Veeran, R.K. Balasundaram, R. Jha, Z. Jaroszewicz, Platinum layers sandwiched between black phosphorous and graphene for enhanced SPR sensor performance. *Plasmonics* **17**(1), 213–222 (2022). <https://doi.org/10.1007/s11468-021-01507-5>
31. B. Karki, A. Uniyal, T. Sharma, A. Pal, V. Srivastava, Indium phosphide and black phosphorus employed surface plasmon resonance sensor for formalin detection: numerical analysis. *Opt. Eng.* (2022). <https://doi.org/10.1117/1.oe.61.1.017101>
32. L. Wu, J. Guo, Q. Wang, S. Lu, X. Dai, Y. Xiang, D. Fan, Sensitivity enhancement by using few-layer black phosphorus-graphene/TMDCs heterostructure in surface plasmon resonance biochemical sensor. *Sens. Actuators B Chem.* **249**, 542–548 (2017). <https://doi.org/10.1016/j.snb.2017.04.110>
33. Y. Jia, Z. Li, H. Wang, M. Saeed, H. Cai, Sensitivity enhancement of a surface plasmon resonance sensor with platinum diselenide. *Sensors (Switzerland)* (2020). <https://doi.org/10.3390/s20010131>
34. H.S. Nugroho, L. Hasanah, C. Wulandari, R.E. Pawinanto, M.H. Haron, A.R.M. Zain, D.D. Berhanuddin, B. Mulyanti, P. Singh, P. Susthitha Menon, Silicon on insulator-based microring resonator and Au nanofilm Kretschmann-based surface plasmon resonance glucose sensors for lab-on-a-chip applications. *Int. J. Nanotechnol.* **17**(1), 29–41 (2020). <https://doi.org/10.1504/IJNT.2020.109348>
35. S. Singh, A.K. Sharma, P. Lohia, D.K. Dwivedi, Ferric oxide and heterostructure BlueP/MoSe₂ nanostructure based SPR sensor using magnetic material nickel for sensitivity enhancements. *Micro Nanostructures* **163**, 107126 (2022). <https://doi.org/10.1016/j.spmi.2021.107126>

Publisher's Note Springer Nature remains neutral with regard to jurisdictional claims in published maps and institutional affiliations.

Springer Nature or its licensor (e.g. a society or other partner) holds

exclusive rights to this article under a publishing agreement with the author(s) or other rightsholder(s); author self-archiving of the accepted manuscript version of this article is solely governed by the terms of such publishing agreement and applicable law.